Cement & Concrete Composites 31 (2009) 705–714

Contents lists available at ScienceDirect

Cement & Concrete Composites

journal homepage: www.elsevier.com/locate/cemconcomp

# A critical examination of statistical nanoindentation on model materials and hardened cement pastes based on virtual experiments

Pavel Trtik, Beat Münch, Pietro Lura *

*Empa, Swiss Federal Laboratories for Materials Testing and Research, Ueberlandstrasse 129, 8600 Dübendorf, Switzerland*

ARTICLE INFO

*Article history:*
Received 3 May 2009
Received in revised form 8 July 2009
Accepted 9 July 2009
Available online 15 July 2009

*Keywords:*
Nanoindentation
Elastic properties
Focused ion beam nanotomography
Composite models

ABSTRACT

Recent results of statistical nanoindentation testing on hardened cement pastes (HCP) reported in the literature show a multipeak response in the elastic modulus frequency plots. These peaks have been interpreted as indicating the true elastic modulus of two calcium silicate hydrate (C–S–H) phases of different densities.

However, the application of statistical indentation for determining material properties of single phases in HCP appears to violate some of the basic principles of the technique. To elucidate this aspect, virtual experiments emulating statistical nanoindentation are performed and presented in this paper. They are based on 3D images of: (i) an idealized two-phase material and (ii) HCP acquired by focussed ion beam nanotomography (FIB-nt); within both 3D images, a marching object is sampled over a large number of positions. Based on the local phase composition within the marching object, a local stiffness is estimated by using simple composite models. Due to the large number of the investigated positions, the elastic modulus can be statistically evaluated in the same manner as in the real statistical indentation experiments.

The results presented in this paper indicate that the homogenous C–S–H regions present in HCP are too small to cause independent and separated peaks in the elastic modulus plots. Moreover, the presence of phases other than C–S–H, namely unhydrated cement and calcium hydroxide, may also produce spurious peaks in the frequency plots. In conclusion, the presented results question the notion that the multipeak signature in statistical nanoindentation experiments on HCP can be explained only by the presence of two distinct C–S–H phases.



## 1. Introduction

According to a model by Jennings [1] which has recently been revised [2], two distinct types of C–S–H are believed to develop in cementitious materials. These two C–S–H types are called low density (LD) C–S–H and high-density (HD) C–S–H. The two C–S–H types differ in the packing configuration of their basic building blocks or globules. While the morphology of the HD C–S–H corresponds to that of closely-packed spheres, the packing of the LD C–S–H is of randomly-packed spheres [1]. According to Jennings [1], the packing of the globules determines the mechanical properties of the two C–S–H phases. It is noticed that C–S–H of different density has been observed for a long time in the cement literature, where the C–S–H was generally subdivided into 'early-product and late-product' or 'inner-product and outer product' (e.g. [3]). Another type of classification of C–S–H into "phenograins and groundmass" was proposed by Diamond and Bonen [4].

An evidence of two C–S–H phases having different mechanical properties was found by Constantinides and Ulm [5] using grid indentation analysis. A further paper by the same authors [6] uses the same technique to confirm the unique nanogranular behaviour of both C–S–H phases.

The existence of two distinct, nanogranular C–S–H phases appears to be a controversial point [7]. Some experimental evidence appears to be at variance with this model. For example, Rößler et al. [8] show low-dose cryo-transmission electron microscopy images of single C–S–H fibres. These images show no evidence of an internal structure of the filament; with additional information from limited-dose electron diffraction, Rößler et al. [8] conclude that the C–S–H shows a sheet silicate-like structure.

Nanoindentation is an experimental technique that provides access to elastic properties of materials [9]. The technique can in principle be used at any lengthscale; the development in measuring techniques over the recent decades allows for standard indentation testing in the nm resolution. The use of nanoindentation for the characterisation of the elastic properties of materials at the nanoscale is ample; this can be deduced from the number of citations of the early pioneering work on nanoindentation [10]. However, it needs to be pointed out here that the underlying theory of indentation testing is based on the assumption of an infinite, homogeneous and isotropic half-space of zero surface roughness

* Corresponding author.
*E-mail address:* Pietro.Lura@empa.ch (P. Lura).

0958-9465/$ - see front matter © 2009 Elsevier Ltd. All rights reserved.
doi:10.1016/j.cemconcomp.2009.07.001

being examined by the indenter; the indenter in addition features an ideal geometrical shape.

The expected surface roughness of HCP was recently estimated [11] using FIB-nanotomography (FIB-nt) [12,13] datasets without the necessity to physically create the surface using the customary sample preparation steps. The results indicated that for samples of HCP with w/c of 0.35, the unaffected surface roughness on the scale relevant for nanoindentation cannot be lower than several hundreds of nanometres. These results shed doubts on the validity of nanoindentation test results with maximum indentation depths in the same order of magnitude (i.e., several hundreds of nanometres). In addition, these results [11] suggest that the very low surface roughness of nanoindentation surfaces that have been reported in literature (e.g. by Miller et al. [14]) may be caused by detritus within the naturally occurring porosity or by collapse of the porosity due to the pressure induced during sample preparation.

The principles of a statistical grid indentation technique were recently reviewed by Constantinides et al. [15]. The principle of statistical indentation is to perform a relatively large number (hundreds) of single indentation tests in a grid and analyze the indentation elastic modulus and hardness with statistical methods. According to [15], the maximum depth, $h_{max}$ (Fig. 1), of the indentation needs to be much deeper than the size of the proposed nanogranular globuli in the representative volume element of the tested material phase, $d_0$. At the same time, $h_{max}$ needs to be much smaller than the size of an average individual region of the material phase that can be considered homogeneous, $D$. How much smaller $h_{max}$ has to be with respect to $D$ depends heavily on the mismatch in elastic modulus of the individual phases. The generally accepted rule-of-thumb in indentation testing of thin films on substrates is that $h_{max}$ has to be smaller than $D/10$ [16]. Investigations of elastic properties of hardened cement pastes usually employ depths between 100 and 500 nm. The volume of material underneath and around the indenter, of which the mechanical properties are probed, is called the interaction volume (Fig. 1). The interaction volume of indentation is directly dependent on the indentation depth, $h_{max}$. Naturally, the shape of the indenter and the microstructure of the material within the interaction volume influence the stress distribution underneath the indenter. However, even though the indentation interaction volume does not have any clear boundary, it is assumed that, for the popularly used Berkovich indenter, the mechanical response of the material stems from a domain approximately 3–4 times larger than $h_{max}$ [5].

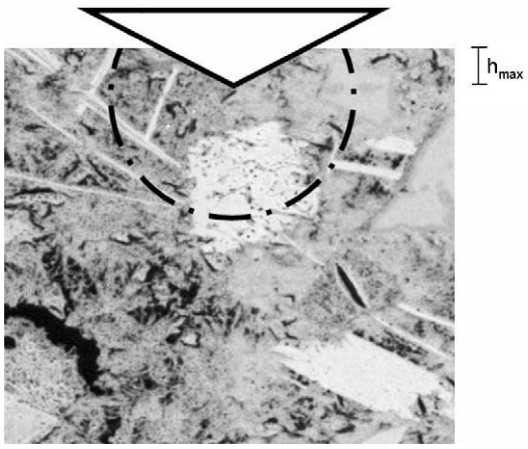


**Fig. 1.** Schematic representation of an indentation in a porous multiphase material. The maximum indentation depth, $h_{max}$, is indicated as well as the influence volume. Notice that depending on the local phase distribution, both $h_{max}$ and the influence volume may vary.

In their paper dealing with the validation of the grid indentation technique, Contantinides et al. [15] perform massive arrays of nanoindentations on a series of two-phase non-porous materials, namely titanium–titanium monoboride alloys (Ti–TiB) with varying amounts of the two phases. The mismatch of the indentation moduli between these two phases was approximately 2.30, with TiB being the stiffer component. These two materials form a non-porous alloy of 70%Ti and 30% TiB with TiB whiskers having characteristic length $D$ equal to 1–3 μm (Fig. 4 in [15]). For this alloy, the histogram of elastic moduli based on nanoindentation shows only one clear peak centred on 144 GPa with a standard deviation of the deconvolved Gaussian peak equal to 12 GPa (Fig. 7b and Table 3 in [15]). No other peak in the elastic moduli histogram has intensity higher than 15% of the mentioned Ti peak. However, the authors appear to have used the knowledge of the elastic moduli of the two phases that are included in the material and therefore they centred at 330 GPa a peak attributed to TiB. This deconvolved Gaussian peak has a standard deviation of 147 GPa, which implies that its 95%-confidence interval (ranging from 36 to 624 GPa) of the Gauss distribution [17] includes all (i.e., also the major peak of the Ti phase) the measured values of elastic moduli (Fig. 7b in [15]). In addition, it can be observed that the above-mentioned histogram actually exhibits also a shoulder peak of approximately five times lower intensity that is centred on approximately 190 GPa, i.e., about 32% higher value than the Ti peak and about 42% lower than the measured value for pure TiB. Obviously, this shoulder peak cannot be attributed to any single phase, since the sample is composed only of Ti and TiB.

It is interesting to compare the above-mentioned experiment reported in [15] with the situation that supposedly exists in hydrated cement paste, i.e., presence of two distinct LD and HD C–S–H phases. The conclusions from the nanoindentation experiments on cement pastes [5] are that two distinct phases of C–S–H with elastic moduli mismatch (about 21 GPa vs. about 29 GPa) occur in the hardened cement pastes with w/c of 0.5. Their volume ratio is approximately 2:1 in favour of LD C–S–H. This volume ratio is very similar to the one of the Ti–TiB alloy [14]. In addition, the elastic moduli of LD and HD C–S–H appear to be much closer than in the case of a Ti–TiB alloy. The occurrence of two or more peaks in the histograms of elastic moduli in cementitious systems is reported in a relatively large number of publications, e.g. [5,6,18,19].

A further interesting point about statistical indentation analysis lies in the problem of separating the valid tests from the entire family of statistical grid indentation test results. In other words, the data obtained by statistical indentation experiments may be filtered or divided into categories based on knowledge gained either from the nanoindentation experiments themselves or from an independent source of evidence, i.e., post-indentation imaging of the indentation sites. The situation differs from investigation to investigation. In some cases [18], it appears that no datapoints obtained by the grid indentation experiment are discarded based on the load–displacement diagram, or at least this step is not reported. In some other cases [6], datapoints that (cit.) "clearly violate the self-similarity of continuum indentation analysis" have been excluded. The authors of [6] add that (cit.) "the largest percentage of discarded curves was related to surface preparation procedures" and that "the number of tests excluded was smaller than 5%". The influence of this exclusion on the elastic modulus frequency plots is supposed to be small, but nevertheless, datapoints appear to have been excluded only on the basis of the nanoindentation response without any confirming evidence from an independent technique.

An alternative approach would be filtering of nanoindentation results based on imaging of the indentation sites. Surprisingly, rather few publications on nanoindentation in HCPs actually show images of the individual indentation sites or images of the

indentation surfaces with resolution relevant for the size of indentations. For example, in a PhD-thesis [20], reporting the results of grid indentation experiments on 48 types of hardened cement pastes, no single image showing the actual nanoindentation imprint is shown. At best, images of the nanoindentation sites in the relevant publications are shown in secondary electron contrast with low resolution [18], while hardly any back-scattered electron images are presented. An exception is [21], in which the authors carried out a limited number of indentations (60) and examined all of them using back-scattered electron imaging. Unfortunately, the results of micromechanical testing are based on indentations of large maximum depths (1500 nm) and therefore the derived elastic moduli in this publication are likely affected by the other phases occurring within the interaction volume underneath the indenter; this fact could be revealed with sufficient resolution only by focused ion beam (FIB) sectioning [22]. Regarding the identification of the phases probed by nanoindentation, an investigation using EDS [18] was recently reported. The images of nanoindentation surfaces (without indentation imprints) show either low porosity [18,23] or, in contrast, rather high surface roughness [5].

As evident from the literature review presented above, some of the very principles on which the application of the grid indentation technique for determining material properties of single phases in HCP is based, appear to be questionable. As a consequence, a set of virtual experiments will be presented hereinafter that, with the inevitable simplifications, attempt at emulating actual grid nanoindentation experiments.

In the first step, a virtual statistical indentation experiment on an idealized two-phase material (3D checkerboard) is performed. The aim of this simulation is to elucidate how small the interaction volume with respect to the size of individual homogeneous islands of material has to be, so that the resulting distribution of the elastic properties is bi-modal.

In a further step, a real FIB-nt dataset of hardened cement paste is used as the three-dimensional input image for a virtual grid indentation analysis. FIB-nt has been recently used to investigate the three-dimensional pore structure of hardened cement pastes with nanoscale resolution [24]. The resolution provided by the 3D image volumes is on lengthscales relevant for the nanoindentation experiments. Based on the local phase composition, a local stiffness is estimated with simple composite models for all virtual indentation sites. Finally, an elastic modulus distribution is calculated based on these virtual volumes that can be compared with the results of nanoindentation experiments. The aim of this virtual experiment is to clarify how the presence of phases with different stiffness and of the porosity generates a multipeak response in the elastic modulus histograms.

## 2. Materials and methods

### 2.1. Input 3D images

#### 2.1.1. Image of a model two-phase material (3D checkerboard)

A virtual 3D image of a model two-phase material was created to investigate the relationship between the sizes of the homogenous isotropic islands, $D$, and the interaction volume of an indenter. In particular, the aim was to find the maximum size of the interaction volume which yields a bimodal distribution of elastic moduli in the resulting histogram. The image consists of $128^3$ voxels. The two material phases occur in this model material in clearly separated domains $D$ of $32^3$ voxels in size (Fig. 2).

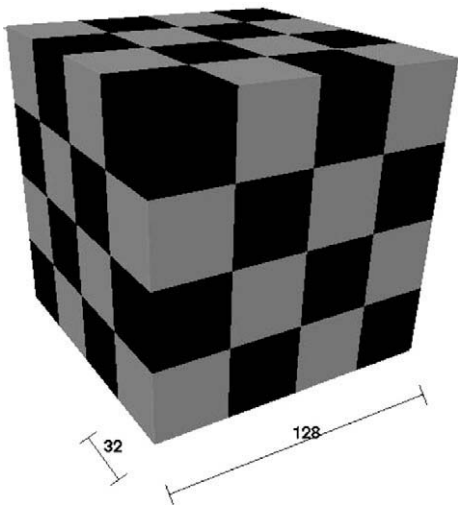


**Fig. 2.** Image of a non-porous two-phase model material for a virtual micromechanical experiment. The size of the image is $128^3$ voxels, while the size of the individual homogeneous material domains $D$ is $32^3$ voxels.

#### 2.1.2. FIB-nt dataset of hardened cement paste

The cement pastes had a w/c 0.30 and were made with CEM I 42.5 Portland cement. The sample of $40 \times 40 \times 160$ mm$^3$ was cast and then demoulded at the age of 1 day. The prism was cured for the first 6 days in tap water at 20 °C, and then transferred to a climatic chamber at 95% RH and 20 °C. At an age of 28 days, samples of dimensions $40 \times 40 \times 10$ mm$^3$ were cut from the centre part of the prism using a diamond saw and hydration was then stopped by freeze-drying. The samples were subsequently epoxy-impregnated and then ground and polished using standard methodology. Smaller samples, approximately 2-mm thick, were cut out from the prisms and glued to an electron microscopy stub. A high-energy ion beam was used to mill a trench around the area of interest in the sample, thus leaving the volume of interest standing out from the bulk sample. Such a prepared volume of interest was then serially sectioned using a low-current ion beam. After completion of each sectioning process, an electron microscopy image of the sectioned surfaces was taken. Further details about sample preparation and data acquisition method are reported elsewhere [25].

FIB-nt is a time- and resources-intensive technique: a single sample may take several days to acquire and analyze. A single FIB-nt site was examined in this investigation, of size $20.4 \times 17.7 \times 6.2$ μm$^3$. The voxel sizes in FIB-nt datasets are given by the magnification factor of the electron microscopy images and, in the slicing direction, by the size of the milled FIB-nt sections. In this particular case, the voxel size was 20 nm, the sectioning distance 40 nm, and the total number of voxels $984 \times 854 \times 155$. This FIB-nt dataset is segmented into three phases: porosity, hydrates and unhydrated cement particles. A 3D representation of the segmented dataset is shown in Fig. 3.

### 2.2. Sampling of interaction volumes for nanoindentation

The virtual experiments described in the following are based on placing an object, representing the interaction volume of a micromechanical test, at various 3D positions within the image volume. This can also be perceived as an object which is virtually marching through the material structure. In order to assess the volume of material affected by nanoindentation, the stresses and strains caused by indentation in the material have to be evaluated. In general, stresses and strains depend both on the indenter (e.g. indenter size and shape, friction between indenter and sample) and on the substrate. For homogeneous, isotropic materials, the exact stresses can be calculated [26]. However, for porous multiphase materials, the size and shape of the volume affected by nanoindentation is much harder to determine, since the local microstructure has

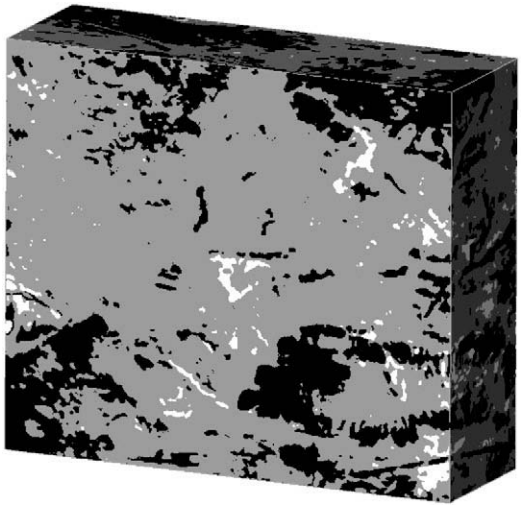

**Fig. 3.** 3D view of the segmented FIB-nt sample. The size of the dataset is $984 \times 854 \times 155$ voxels, representing a volume of $20.4 \times 17.7 \times 6.2$ μm$^3$. The porosity is white, the hydrates are gray and the unhydrated particles are black.

considerable influence on the deformation response. If the same maximum load of indentation is specified in a real grid indentation experiment, the maximum depth of the indentation, and hence the size of the interaction volume, depends in reality on the hardness of the investigated spot. As a result, an exact definition of the size and shape of the marching object in the virtual experiments is not possible and some simplifications have to be introduced.

In the case of the model two-phase material (as described in Section 2.1.1), cubes of various sizes are taken as interaction volumes. The sizes of such marching cubes were varied as:

$$m = 2^n, \quad n = \{1, 2, \ldots, 5\} \text{ (i.e. } m = 1, 2, 4, 8, 16, 32).$$

The marching object was sampled over $2^{21}$ positions (needless to say, many of them self-similar) for each size of $m$. The volume fractions of the two phases were evaluated for each position and this served as an input for the calculation of the composite elastic modulus within the interaction volume (see Section 2.3). In order to refine the search, sizes of $m$ equal to 10, 12 and 14 voxels were analysed as well.

In the case of the FIB-nt dataset, cubes of 1-μm edge were considered as the interaction volume. This interaction volume corresponds to an indentation depth $h_{max}$ of about 250–330 nm, based on the assumption that the interaction volume is 3–4 times larger than the indentation depth [5]. The size of the interaction volume remained the same for all the positions of the interaction volumes, thus disregarding the influence of the material microstructure on the depth of indentation. In order to avoid statistical dependency of individual interaction volumes, the 1-μm cubes were sampled within the microstructure of the hardened cement paste at a distance of about 2 μm in the three directions (a 3D grid), see Fig. 4. A dataset of 280 cubes, each representing a different indentation site, was obtained with this procedure. Once the set of the valid cubes is determined, the volume fractions of porosity, hydrates and unhydrated cement are evaluated for each cube.

### 2.3. Estimation of the local elastic moduli from the 3D images of interaction volumes

#### 2.3.1. Influence of porosity

It has been long known that porosity is the major factor in controlling the elasticity of Portland cement systems [27]. Different empirical formulae connecting the elastic modulus and porosity have been devised, for example [28]:

$$E = E_0 \cdot e^{-bp} \tag{1}$$

where $E$ is the elastic modulus, $E_0$ is the modulus of non-porous material, $b$ is a constant that depends on the shape of the pores and $p$ is the porosity.

Another form taken by this relationship is:

$$E = E_0 \cdot (1 - p)^3 \tag{2}$$

Eq. (2) has been used successfully for porous ceramics and cement paste [29–31].

It is first assumed that the entire solid skeleton (composed of hydration products and unhydrated cement) has no variation in the elastic modulus. The local elastic modulus at each indentation site (i.e., within a cube with 1-μm side) can then be calculated with Eq. (2). For the choice of $E_0$, either an arbitrary value can be assumed, so that the results can be presented only as a variation of elastic properties, or a realistic value for the elastic modulus of C–S–H can be derived from the literature. The main source for the elastic modulus of C–S–H is nanoindentation [5]. Following Haecker et al. [32] $E$ = 22.4 GPa is estimated for C–S–H, based on the previously-cited nanoindentation results and on Helmuth and Turk [33]; furthermore, a Poisson ratio $\nu$ = 0.25 is assumed [32].

#### 2.3.2. Influence of the composition of the solid skeleton

The elastic properties of a solid composed of a matrix and inclusions can be calculated with a model proposed by Kuster and Toksöz [34].

$$\frac{K_c}{K_m} = \frac{1 + [4G_m(K_s - K_m)/(3K_s - 4G_m)K_m]c}{1 - [3(K_s - K_m)/(3K_s - 4G_m)]c} \tag{3}$$

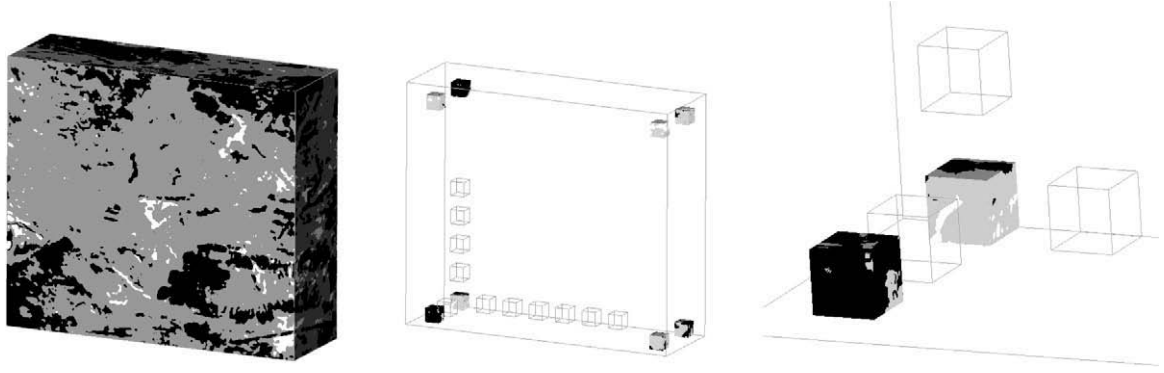

**Fig. 4.** 3D view of the FIB-nt sample (left). Scheme of the principle of a virtual grid indentation experiment, with only the corner cubes of the 3D grid shown in full (centre). Detail of two 1-μm cubes representing a nanoindentation interaction volume (right).

$$\frac{G_c}{G_m} = \frac{(6K_m + 12G_m)G_s + (9K_m + 8G_m)[(1-c)G_m + cG_s]}{(9K_m + 8G_m)G_m + (6K_m + 12G_m)[(1-c)G_s + cG_m]} \quad (4)$$

where $K_c$ and $G_c$ are, respectively, the bulk and the shear modulus of the composite comprising hydration products and unhydrated cement particles; $K_m$ and $G_m$ are, respectively, the bulk and the shear modulus of the hydration products; $K_s$ and $G_s$ are, respectively, the bulk and the shear modulus of the unhydrated cement particles; $c$ is the volume concentration of the unhydrated cement particles.

Once $K_c$ and $G_c$ are known, the elastic modulus of the composite can be calculated according to the theory of elasticity:

$$E_c = \frac{9K_cG_c}{3K_c + G_c} \quad (5)$$

The Kuster and Toksöz model has shown to provide good predictions of the elastic properties of mortars, where the matrix is represented by cement paste and the inclusions by sand grains [35].

In the case of the model specimen (3D checkerboard, Fig. 2), no porosity is present. Therefore, the local elastic properties stem from the material properties of the individual solid components. To the two phases of this model material, elastic properties found in the literature for LD C–S–H and HD C–S–H phases [5] have been assigned. The chosen elastic moduli and Poisson's ratios are as follows: $E_{LD}$ = 21 GPa, $E_{HD}$ = 29 GPa and a Poisson's ratio of 0.25 for both phases, which leads to bulk and shear moduli of (14.0 GPa and 8.4 GPa) and (19.3 and 11.6 GPa) for our model LD and HD phases, respectively. Eqs. (3)–(5) are then used to calculate the elastic modulus of the composite within the interaction volume of a nanoindenter (see Section 2.2). The geometry of a 3D checkerboard differs from the one assumed by the Kuster and Toksöz model [34]; however, this model is used in this study as a first approximation to allow easy calculation of the elastic properties of the composite. More sophisticated models may be used in the future when precise quantitative results are needed.

For the FIB-nt dataset (Fig. 3), the solid skeleton is considered as composed of unhydrated cement and hydration products. Following Haecker et al. [32] (based on [36]), the elastic properties of the unhydrated cement are taken as $E_{UC}$ = 117.6 GPa and $\nu_{UC}$ = 0.314 ($K_{UC}$ = 105.2 GPa and $G_{UC}$ = 44.8 GPa). Also in the case of the FIB-nt datasets, the use of the Kuster and Toksöz model [34] is not fully justified, and should be considered only a first approximation within the scope of the present investigation. In fact, in the case of a cement paste at the magnification accessed by FIB-nt, unhydrated cement grains are not completely embedded into hydration products, nor are they small compared to the interaction volume considered.

#### 2.3.3. Combined influence of porosity and unhydrated cement in FIB-nt datasets

In the case of the FIB-nt dataset, and only for interaction volumes containing both porosity and solid matter, the elastic modulus is calculated with the following equation:

$$E = E_c \cdot (1-p)^3 \quad (6)$$

where $E_c$ is the elastic modulus of the composite composed of hydration products and unhydrated cement particles, calculated with Eq. (5). This approach can be considered a first approximation, since Eq. (6) is supposed to be valid in the case of pores much smaller than the overall volume of the composite. Also in this case, it is expected that a finite element model would yield more precise quantitative results.

#### 2.3.4. Frequency plots

A relative frequency plot is a graphical data analysis technique for summarizing the distributional information of a variable. The response variable is first divided into equal sized intervals (or bins). The number of occurrences of the response variable, divided by the total number, is then calculated for each bin. The frequency plot then consists of the relative frequencies on the ordinates and of the response variable (i.e., the mid-point of each interval) on the abscissas. Once the elastic modulus of a set of possible indentation sites is calculated with Eq. (6), relative frequency plots of the elastic modulus can be constructed by assigning a bin size to the elastic modulus data set and plotting the results as explained above. In the analysis of nanoindentation results obtained by experiments, variable sizes of bins are generally used: for example, the size of the bins varies from 2 GPa [18] to 2.5 GPa [6] to 5 GPa [37]. It is noticed that changing the size of the bin leads to a modification of the relative frequency plots; the overall frequencies become lower with smaller bins and possibly the shape and the number of the peaks may change.

## 3. Results

### 3.1. Model two-phase material (3D checkerboard)

The results of the virtual micromechanical experiments for some chosen dimensions of the interaction volumes are presented in Fig. 5. It can be noted that the bi-modality of the distribution of elastic modulus disappears completely for a size of the cube $D$ of $12^3$ voxels, while for the size of $10^3$ voxels, the bi-modality can still be deduced. In other words, the results reveal that, if the grid indentation method is performed in a purely statistical way, that is, without any foreknowledge of the indentation spot, the evidence of a bi-modality in the histograms disappears, if the size of the indentation interaction volume exceeds about 4% per cent of the volume of homogeneous domains. Equivalently, one could say that the homogeneous domains should have a volume at least 25 times larger than the interaction volume of the indenter, or have a linear size at least three times larger, in order to yield a bimodal distribution in a frequency plot. It must be highlighted here that the model material, on which this calculation was performed, can likely be considered as a close-to-optimum geometrical environment for assessment of appearance of bimodal distribution of the elastic modulus. In other words, all the additional instability aspects of micromechanical testing on real materials will likely cause the bimodal distribution to disappear even if smaller interaction volumes are used.

Another interesting observation is that, starting at a size of the cube $D$ of $10^3$ voxels, and then more evidently for $12^3$ and $16^3$ voxels, a peak appears at an elastic modulus of 25 GPa. This peak does not correspond to any phase present in the model material and instead shows a stiffness which is the average value between the two phases (with modulus 21 and 29 GPa). For a size of the interaction volume $D$ of $32^3$ voxels, corresponding to the size of the homogenous single-phase domains (Fig. 2), the peak at 25 GPa dominates the elastic modulus histogram, while no peaks are visible at 21 and 29 GPa. It is therefore clear that depending on the respective sizes of the homogenous domains and the interaction volume, peaks may appear in the elastic modulus histogram that do not correspond to the stiffness of any of the phases present in the microstructure.

### 3.2. FIB-nt dataset of HCP

The phase composition (i.e., porosity, unhydrated cement and hydration products) of 280 individual cubes of dimension $1 \times 1 \times 1\ \mu m^3$ sampled from the prismatic sample (see Section 2.1.2) is shown in Fig. 6. It is noticed that unhydrated cement

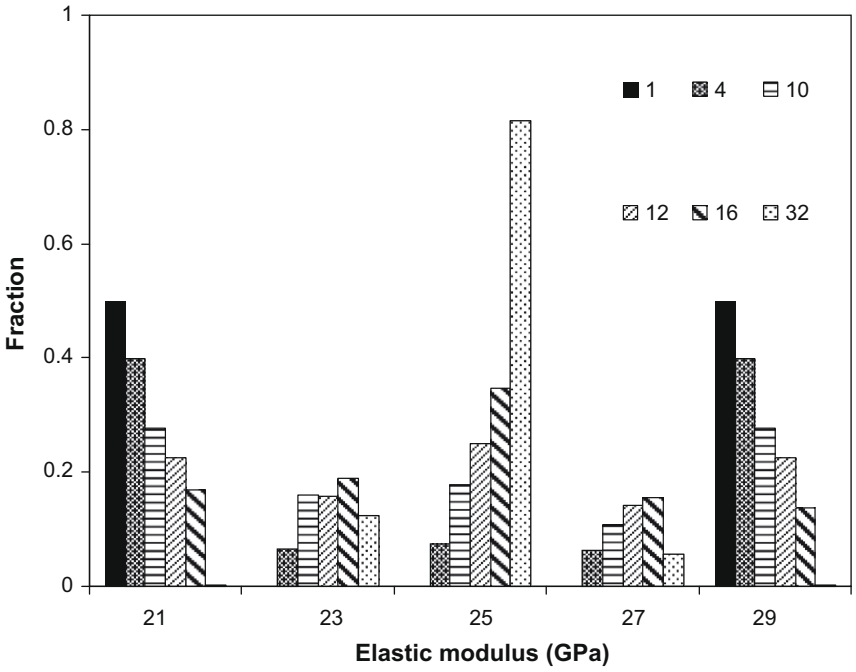


**Fig. 5.** Histograms of composite elastic moduli from the 3D image of a model non-porous two-phase material (see Fig. 2) for size of the interaction volumes $D$ of 1, 4, 10, 12, 16 and 32 voxels cubed. Note that the bi-modality of the distribution disappears completely for the size of the cube of $12^3$ voxels.

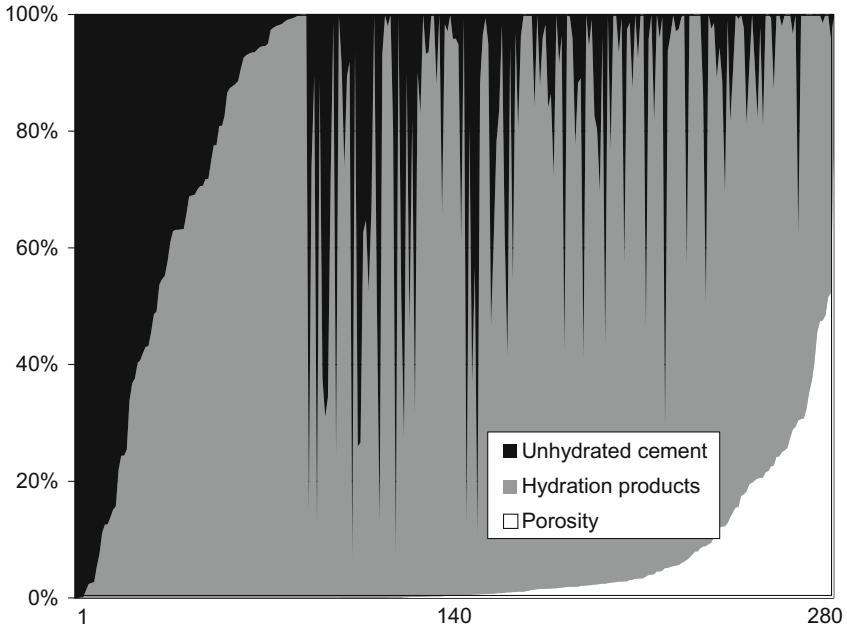


**Fig. 6.** Phase composition of 280 sampled 1 $\mu m^3$ cubes.

and hydration products within the single cubes may vary from 0% to 100%, while the porosity varies from 0% to 78%.

The frequency plots were calculated according to the procedure described in Section 2.3.4, while the local elastic modulus for the indentation sites (single cubes with 1-μm edge) was calculated based on the procedure described in Sections 2.3.1 to 2.3.3. Fig. 7 shows frequency plots calculated according to different models; the bin size is 1 GPa. The first model considers a two-phase material composed of hydration products and porosity, where the elastic modulus of the composite is calculated with Eq. (2). To apply this model, all the solids were considered to possess the elastic modulus of hydration products. As evident from Fig. 7, a single peak with relative frequency of 0.546 appears at 22.5 GPa, corresponding to the assumed elastic modulus (22.4 GPa) of the hydration products (see Section 2.3.1). The peak appears to extend to about 17.5 GPa, with a cumulated frequency of 0.83. For lower values of the modulus, no distinct peaks higher than about 0.02 appear. The second model considers another two-phase material composed of hydrated products and unhydrated cement only, where the elastic properties of the composite are calculated with Eq. (5). Also in this case (Fig. 7), a peak appears at 22.5 GPa, with a broad shoulder; a number of secondary peaks are evident in the region from 26 to 38 GPa. On the contrary, no special peak appears at 117.7 GPa, which corresponds to the modulus of

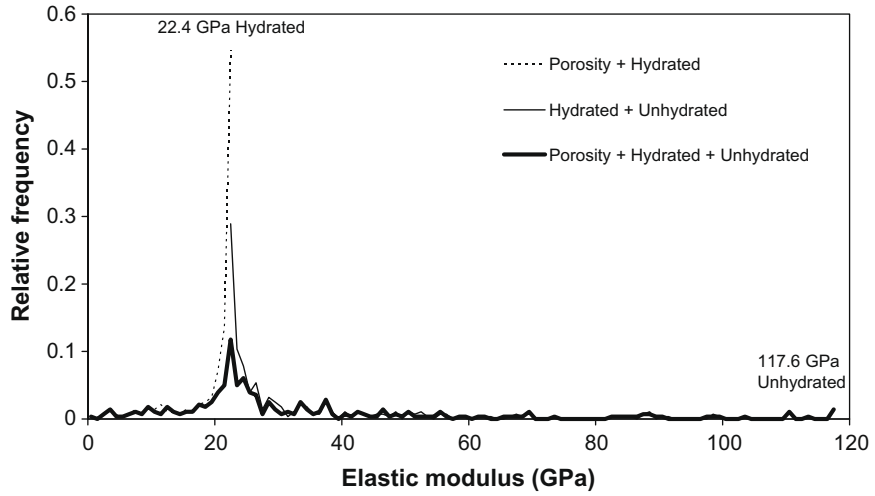


**Fig. 7.** Elastic modulus frequency plots, calculated taking into account only the effect on the elastic modulus of the porosity, the effect of unhydrated cement, or both.

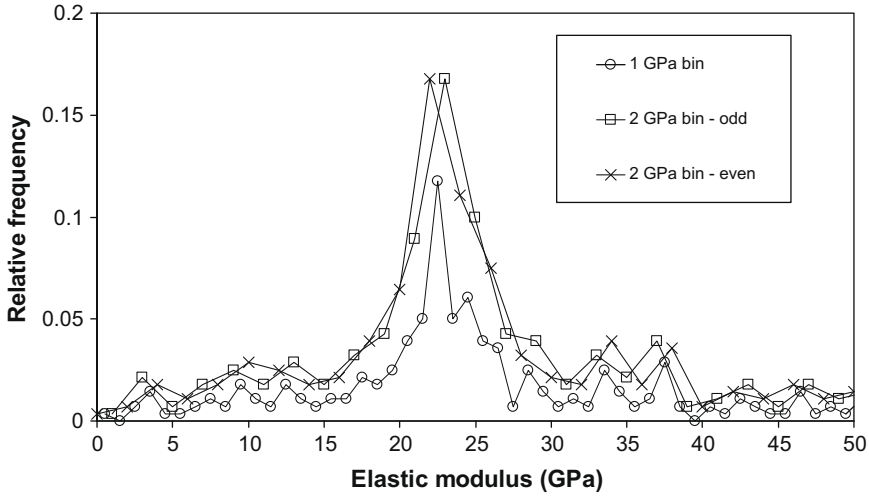


**Fig. 8.** Elastic modulus frequency plots calculated taking into account both porosity and unhydrated cement (Eq. (6)); effect of varying the size and position of the bins.

unhydrated cement. This reflects the fact that only a few cubes with 100% unhydrated cement are included in the dataset.

The third model considers a 3-phase material where the elastic modulus is calculated with Eq. (6). It can be considered as a combination of the two previous models, in which the elastic modulus of the solid phases is calculated first and in a second step the influence of porosity is considered. This model produces a main peak (Fig. 7) at 22.5 GPa, which decreases smoothly for lower values. For higher values of the modulus, secondary peaks appear between 24 and 38 GPa. These secondary peaks have heights that range from 1/2 to 1/5 of the main peak. It is noticed that these multiple peaks of comparable height have been generated by the presence of unhydrated cement (with elastic modulus 117.7 GPa), hydration products (modulus 22.4 GPa) and porosity in various amounts, while no materials with elastic modulus in the range 24–38 GPa were included in the simulation. This result appears to substantiate the assumption that random peaks in the elastic modulus frequency plots may be generated by the distribution of the phases, rather than indicating the presence of a phase with a specific elastic modulus within the region of the peak.

Fig. 8 shows the effect on the relative frequency plots of the size of the bins (1 and 2 GPa) and of their position. Increasing the size of the bins leads to higher relative frequency values and to a broadening of the peaks. At the same time, the choice of the bins produces a slight shift of the main peak. Moreover, according to the size of the bins and their position, smaller peaks may be joined into a larger one.

## 4. Discussion

### 4.1. Dimension of homogeneous C–S–H regions

As was mentioned above (Section 2.2), the nanoindentation experiments on HCP reported in the literature utilise maximum indentation depths resulting in probed volumes of approximately 1 $\mu m^3$. The results of Fig. 5 show that for a model 2-phase material, the interaction volume should have a linear size at least three times smaller than the size of homogeneous isotropic domains; if this condition is not fulfilled, no bi-modal distribution appears in the elastic modulus histograms. Therefore, for HCP to fulfil this condition, homogeneous isotropic regions of either LD or HD C–S–H with edge length larger than about 3 μm should be present, so that a bimodality in the distribution of elastic properties of C–S–H is revealed.

Any such large homogenous C–S–H regions should be also evident in 2D in scanning electron microscopy images of a HCP. As an example, a scanning electron microscopy image of HCP (Portland cement, w/c of 0.3) based on low-keV back-scattered signal is

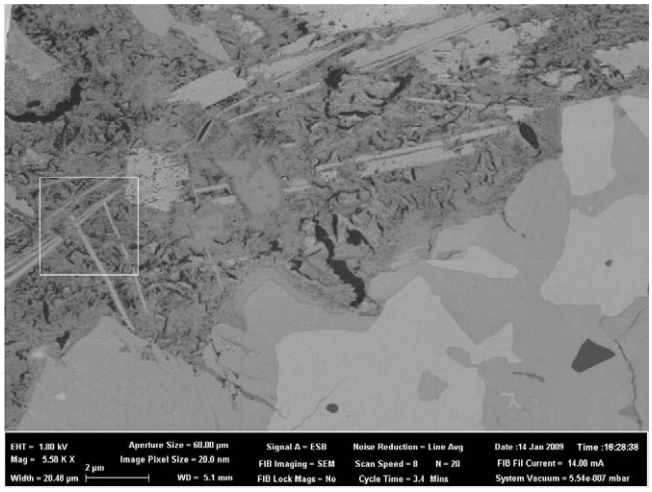


**Fig. 9.** Example of low-keV BSE image of hardened cement paste. A square of about 3 μm is superimposed to the image (centre left of the image). No homogeneous domains of hydration products of such size have been found in the image.

shown in Fig. 9. This image does not exhibit any large homogeneous domain of hydrated phases. This is well in line with the conclusions by Richardson and Groves [38] based on investigations of chemical composition of C–S–H gels using microprobe analysis and TEM. They state that (cit.) "...single phase Op [outer product] C–S–H rarely occurs in mature hardened OPC paste in volumes greater than approximately 2 $\mu m^3$" [38].

### 4.2. Other phases

In cement paste, a number of phases other than C–S–H and unhydrated cement are present. For example, Lothenbach et al. [39] showed that a mature Portland cement paste with w/c 0.4 contained about 50% C–S–H, 20% portlandite, 10% ettringite, 12% monocarbonate, 1% calcite, 3% unhydrated cement and 4% porosity by volume. This means that purely on a statistical basis, even if an indenter were small enough to probe individual phases of a cement paste, about 50% of the time the indenter should be probing phases other than C–S–H.

#### 4.2.1. Portlandite

Portlandite occurs in the structure of HCP in a number of forms with the sizes of its structural features spanning several orders of magnitude. According to [40], portlandite may be present as 1–10 nm occluded CH-like material within C–S–H, as thin elongated platelets of 10–100 nm in thickness, and as large CH domains of high geometrical complexity of tens of micrometres in size.

From a micromechanical perspective, portlandite crystals have a higher elastic modulus compared to C–S–H and moreover their elastic modulus depends on the direction of loading, ranging from 22.6 to 99.4 GPa [41]. If the portlandite crystals are oriented randomly in the cement paste, in about 2/3 of the cases their elastic modulus will be comprised between 22.6 GPa (the minimum) and 36.3 GPa (the value at 0°).

#### 4.2.2. Ettringite, calcite and monocarbonate

Elastic modulus of ettringite has been recently derived for natural ettringite crystals with Brillouin spectroscopy [42]. Depending on the orientation of the crystals and the direction of loading, the elastic modulus varies from 20 to 40 GPa.

The amount of calcite present in the majority of modern Portland cements, up to 5% of cement weight, has an impact on the phase composition of a mature cement paste. A small amount of calcite will be present in the hydrated cement paste, for which an elastic modulus of 79.6 GPa [32] is reported. More important, a substantial amount of monocarbonate is expected to be formed [39], which should have elastic properties similar to CH [32].

Depending on their size distribution, these and other minor components of hardened cement pastes may also have the potential to introduce spurious peaks in the 'nanoindentation signature' of hardened cement pastes.

### 4.3. Representativeness of the FIB-nt results

As previously mentioned, results obtained based on a single FIB-nt volume (of size $20.4 \times 17.7 \times 6.2\ \mu m^3$) might be considered with suspicion, as they might not be representative of the average properties of a cement paste. However, the total amount of porosity based on FIB-nt has been shown to be in satisfactory agreement with porosity measured by MIP on the same cement paste [24], when only pores larger than the resolution of the FIB-nt images are considered. Even if the phase composition of the FIB-nt volume is not exactly representative of a cement paste, this should only be reflected into the respective height of the peaks in the elastic modulus frequency plots (Fig. 7), while the main conclusions of this analysis should remain unaltered.

Another issue of interest is whether the sampling method used to select the interaction volumes leads to statistically independent indentation sites [6]. In other words, choosing cubes that are too close to each other in the cement paste might introduce some statistical bias in the sample.

Both these issues could be solved in future work by examining a number of different FIB-nt volumes or possibly larger volumes, where the indentation sites can be sampled randomly at a larger distance through the microstructure.

### 4.4. Elastic modulus calculations

A simple procedure was used for the calculation of the elastic moduli of the single indentation volumes (see Section 2.3). Originally, the composite models used were developed for cases in which both the pores and the hard inclusions (unhydrated cement) are much smaller than the volume of interest; this is obviously not the case for a cement paste at this level of magnification. Moreover, the interaction volume of an indentation may vary depending on the phases encountered. For instance, if a large pore is present on the indented surface, the indenter may dig deeper into the cement paste and the interaction volume might be larger.

A strategy to refine the calculation of the local elastic modulus would be assessing the elasticity of the materials directly from the 3D images. Significant work has been carried out in this area by Garboczi and Day [43], who developed a finite element technique where the equations of elasticity are solved on a finite element mesh that is constituted by a lattice superimposed to a 3D digital image. Further work on computation of linear elastic properties from tomographic images was performed by Arns et al. [44]. This approach may be attempted in the future for calculating the local elastic modulus in virtual statistical nanoindentation experiments.

### 4.5. Elastic modulus frequency plots

As evident from Fig. 7, while the main peak due to C–S–H always occurs around the expected value of 22.4 GPa, multiple spurious peaks may be introduced in the region 30–40 GPa by the presence of different amounts of unhydrated cement within the volume of influence of one indenter. It is noticed that these peaks, albeit lower, appear in the same regions where peaks were observed by e.g. Constantinides and Ulm [5] and Zhu et al. [18]. In addition, in real cement pastes both calcium hydroxide and other

hydrate phases (see Section 4.2) may produce peaks in the same region. In particular, calcium hydroxide alone may constitute about 20% by volume of a mature cement paste with high w/c [39] and has an elastic modulus in the range 22–36 GPa. It is the opinion of the authors that, considering this evidence, the identification of the peaks found in, e.g., [5,6,18,19] with HD and LD C–S–H should be reconsidered. In particular, it is suggested that the peak interpreted as belonging to LD C–S–H could indicate the presence of a single C–S–H phase, while the HD peak could be a spurious peak due to presence of other phases, namely unhydrated cement, CH and other crystalline hydration products, within the influence volumes of the indenter.

A further consideration is that the size and the position of the bins in the relative frequency plots may influence the position and the sizes of the peaks that are detected (Fig. 8). In the literature, the bins appear to vary both in size and in position [6,18,37]. In the results presented in this study, increasing the number of bins increases the number of peaks; moreover, even a small shift (e.g. by a fraction of the bin size) of the bin positions at the same number of bins leads to a redistribution of the peak positions. In later work on nanoindentation [45], attempts are in fact made to overcome the bias introduced by the arbitrary choice of the bins and peaks are instead directly extracted from the cumulative curves.

### *4.6. General remarks on the usefulness of nanoindentation for assessing the local mechanical properties of porous disordered materials at the nanoscale*

Nanoindentation is a useful technique for determination of elastic properties of homogeneous materials or heterogeneous materials with layered structures [46]. As explained in this investigation, for the assessment of the mechanical properties of individual phases in porous heterogeneous materials, the statistical grid indentation technique may be less suitable.

A requirement for nanoindentation is that the surface roughness of the cement paste to be indented should be a fraction of the maximum indentation depth. This requirement is difficult or impossible to fulfil for a normal cement paste, since its natural porosity will result in a roughness at the surface of the order of magnitude of 300 nm [11]. Consequently, the surface roughness of a cement paste imposes a lower limit to the dimension of the indentation depth, which should be much larger than 1 μm. Hardly any of the statistical indentation investigations reported in the literature use such large maximum indentation depths.

At the same time, as discussed in Section 4.1, no homogenous region of outer-product C–S–H with volume larger than about 2 $\mu m^3$ are normally observed in a cement paste (see [38] and Fig. 9). As shown in Section 3.1, in order to obtain a bimodal distribution in an elastic modulus frequency plot, the interaction volume of the indenter should have an edge smaller than about 1/3 of the homogenous regions. This means that the linear size of the interaction volume should be at least smaller than about 0.6 μm, or equivalently, that the indentation depth should be smaller than about 150–200 nm.

These two conditions are clearly in contradiction, at least for a normal cement paste. Possible solutions for using a statistical grid indentation technique would be constructing artificial systems [47] where the porosity is lower or the surface roughness smaller, for example special compacts of hydration products. Alternatively, the homogenous islands of C–S–H should be larger. However, it would then be questionable, if the composition and the mechanical properties of phases in these systems would correspond to the phase composition in a real cement paste.

In the authors' opinion, the indentation technique may be possibly useful for assessment of mechanical properties of hydrated compounds of HCPs when the following conditions are met:

(i) the material microstructure within each individual interaction volume can be assessed (or at least with high degree of confidence estimated) and thus the occurrence of a homogeneous isotropic material phase within the interaction volume can be assured;
(ii) the surface roughness at the indentation site is a small fraction of the maximum indentation depth and the preparation steps for the production of indentation surfaces do not change the mechanical properties of individual phases.

These conditions can possibly be met, if a nanoindentation device is tailor-made for use within a high-resolution imaging device, e.g. by an in situ ESEM nanoindenter. In such a device, the indentation site can be deliberately placed within sufficiently large domains of homogeneous material and the surface roughness can be assessed with sufficient resolution.

## 5. Conclusions

Virtual experiments that emulate statistical nanoindentation experiments were performed. They were based on 3D images of: (i) an idealized two-phase material and (ii) HCP acquired by focussed ion beam nanotomography (FIB-nt), in which a marching object was sampled over a large number of positions. Based on the local phase composition within the marching object, a local stiffness was estimated with simple composite models. Due to the very large number of the investigated positions, the elastic moduli could be statistically evaluated in the same manner as in the real statistical indentation experiment.

The results based on the image of an idealized two-phase material show that the linear size of the nanoindentation interaction volume has to be at least three times smaller than the homogeneous isotropic domains of a single phase, in order for the histograms of elastic modulus to show a bimodal distribution. If this requirement is not met, a spurious single peak appears at an elastic modulus corresponding roughly to the average of the moduli of the phases. Having assumed the usual maximum indentation depth utilised in statistical nanoindentation experiments (about 300 nm), the linear size of such regions has to be larger than about 3 μm. BSE images of HCP show that hardly any such regions of C–S–H exist in the microstructure of HCP.

The results based on the FIB-nt dataset reveal that the elastic modulus histograms show multiple peaks even in the case of a material that is segmented into three phases only (porosity, hydrated and unhydrated phases), i.e., without the hydrated phase being composed of different types of distinct hydration products. The presence of unhydrated cement produces peaks in the 30–40 GPa region, which is far lower than their own elastic modulus. It is concluded that the peaks that are identified in the literature as belonging to LD and HD C–S–H could in reality equally reflect the presence of only one type of C–S–H next to other crystalline phases of high elastic moduli (e.g., unhydrated cement, calcium hydroxide) within the indentation interaction volume.

In general, the results of this study question the application of statistical nanoindentation to HCP and call for a critical examination of the technique.

## Acknowledgements

The authors thank Dale Bentz, Andreas Leemann and Barbara Lothenbach for critical reading of the manuscript and Ellis Gartner for useful discussion.

## References


[1] Jennings HM. A model for the microstructure of calcium silicate hydrate in cement paste. Cem Concr Res 2000;30:101.
[2] Jennings HM. Refinements to colloid model of C–S–H in cement: CM-II. Cem Concr Res 2008;38(3):275–89.
[3] Groves GW, Lesueur PJ, Sinclair W. Transmission electron-microscopy and microanalytical studies of ion-beam-thinned sections of tricalcium silicate paste. J Am Ceram Soc 1986;69:353.
[4] Diamond S, Bonen D. Microstructure of hardened cement paste – a new interpretation. J Am Ceram Soc 1993;76(12):2993–9.
[5] Constantinides G, Ulm FJ. The effect of two types of C–S–H on the elasticity of cement-based materials: test results from nanoindentation and micromechanical modeling. Cem Concr Res 2004;34(1):67–70.
[6] Constantinides G, Ulm FJ. The nanogranular nature of C–S–H. J Mech Phys Solids 2007;55:64.
[7] Beaudoin JJ, Alizadeh R. A discussion of the paper ''Refinements to colloidal model of C–S–H in cement: CM-II" by Hamlin M. Jennings. Cem Concr Res 2008;38:1026.
[8] Rößler C, Stark J, Steiniger F, Tichelaar W. Limited-dose electron microscopy reveals the crystallinity of fibrous C–S–H phases. J Am Ceram Soc 2006;89(2):627–32.
[9] Doerner MF, Nix WD. A method for interpreting the data from depth-sensing indentation instruments. J Mater Res 1986;1(4):601–9.
[10] Oliver WC, Pharr GM. An improved technique for determining hardness and elastic-modulus using load and displacement sensing indentation experiments. J Mater Res 1992;7:1564–83.
[11] Trtik P, Dual J, Muench B, Holzer L. Limitation in obtainable surface roughness of hardened cement paste: 'virtual' topographic experiment based on focussed ion beam nanotomography datasets. J Microsc Oxford 2008;232:200.
[12] Inkson BJ, Steer T, Mobus G, Wagner T. Subsurface nanoindentation deformation of Cu–Al multilayers mapped in 3D by focused ion beam microscopy. J Microsc Oxford 2001;201:256.
[13] Holzer L, Indutnyi F, Gasser P, Münch B, Wegmann M. Three-dimensional analysis of porous $BaTiO_3$ ceramics using FIB nanotomography. J Microsc 2004;216(1):84–95.
[14] Miller M, Bobko C, Vandamme M, Ulm FJ. Surface roughness criteria for cement paste nanoindentation. Cem Concr Res 2008;38:467.
[15] Constantinides G, Chandran KSR, Ulm FJ, Van Vliet KJ. Grid indentation analysis of composite microstructure and mechanics: principles and validation. Mater Sci Eng Struct Mater Prop Microstruct Process 2006;430:189.
[16] Bückle H. VDI Ber 1961;41:14.
[17] de Moivre A. Approximatio ad Summam Terminorum Binomii $(a+b)n$ in Seriem expansi (printed on 12 November 1733 in London for private circulation). Reprinted in: Archibald RC. A rare pamphlet of Moivre and some of his discoveries. Isis 1926;8:671–83.
[18] Zhu W, Hughes JJ, Bicanic N, Pearce CJ. Nanoindentation mapping of mechanical properties of cement paste and natural rocks. Mater Charact 2007;58:1189.
[19] Sorelli L, Constantinides G, Ulm FJ, Toutlemonde F. The nano-mechanical signature of ultra high performance concrete by statistical nanoindentation techniques. Cem Concr Res 2008;38:1447.
[20] Vandamme M. The nanogranular origin of concrete creep: a nanoindentation investigation of microstructure and fundamental properties of calcium–silicate–hydrates. PhD thesis, MIT, Boston, USA; 2008.
[21] Hughes JJ, Trtik P. Micro-mechanical properties of cement paste measured by depth-sensing nanoindentation: a preliminary correlation of physical properties with phase type. Mater Charact 2004;53:223.
[22] Trtik P, Reeves CM, Bartos PJM. Use of focused ion beam (FIB) for advanced interpretation of microindentation test results applied to cementitious composites. Mater Struct 2000;33:189.
[23] Němeček J, Kopecký L, Bittnar Z. Nanoidentation size effect of cement pastes 2nd international symposium on nanotechnology in construction. Bagneux: Rilem Publications s.a.r.l.; 2005. p. 1–7.
[24] Münch B, Holzer L. Contradicting geometrical concepts in pore size analysis attained with electron microscopy and mercury intrusion. J Am Ceram Soc 2008;91(12):4059–67.
[25] Holzer L, Gasser P, Muench B. Quantification of capillary pores and Hadley grains in cement pastes using FIB-nanotomography. In: Konsto-Goloutos MS, editor. Proc. ECF 16, Alexandroupolis, Greece, measuring, monitoring and modelling concrete properties. Dordrecht: Springer; 2006. p. 509–16.
[26] Fischer-Cripps AC. Nanoindentation. 2nd ed. New York: Springer; 2004. 290 p.
[27] Feldman RF, Beaudoin JJ. Microstructure and strength of hydrated cement. Cem Concr Res 1976;6:389–400.
[28] Sereda PJ. Significance of microhardness of porous inorganic materials. Cem Concr Res 1972;2:717–29.
[29] Powers TC. Fundamental aspects of shrinkage of concrete. Rev Matér 1961;544:79.
[30] Kendall K, Howard AJ, Birchall JD. The Relation between porosity, microstructure and strength, and the approach to advanced cement-based materials. Phil Trans Roy Soc Lond A 1983;310:139–53.
[31] Zech B, Setzer MJ. The dynamic elastic modulus of hardened cement paste. Part I: a new statistical model-water and ice filled pores. Mater Struct 1988;21:323–8.
[32] Haecker CJ, Garboczi EJ, Bullard JW, Bohn RB, Sun Z, Shah SP, et al. Modeling the linear elastic properties of Portland cement paste. Cem Concr Res 2005;35:1948–60.
[33] Helmuth RA, Turk DH. Elastic moduli of hardened Portland cement and tricalcium silicate pastes: effect of porosity. In: Symposium on structure of Portland cement paste and concrete (special report 90), Highway Research Board, Washington, DC; 1966. p. 135–44.
[34] Kuster GT, Toksöz MN. Velocity and attenuation of seismic waves in two-phase media. Part I: theoretical formulations. Geophysics 1974;39:587.
[35] Zimmermann RW, King MS, Monteiro PJM. The elastic modulus of mortar as a porous-granular material. Cem Concr Res 1986;16:239–45.
[36] Velez K, Maximilien S, Damidot D, Fantozzi G, Sorrentino F. Determination by nanoindentation of elastic modulus and hardness of pure constitutents of Portland cement clinker. Cem Concr Res 2001;31:555–61.
[37] Ulm FJ, Delafargue A, Constantinides G. Experimental microporomechanics. Lecture notes prepared for the summer school 'Applied Micromechanics of Porous Materials', Coordinated by L. Dormieux and F.-J. Ulm, International Centre for Mechanical Sciences (CISM), Udine, Italy, July 19–23; 2004.
[38] Richardson IG, Groves GW. Microstructure and microanalysis of hardened ordinary portland-cement pastes. J Mater Sci 1993;28:265.
[39] Lothenbach B, Le Saout G, Gallucci E, Scrivener K. Influence of limestone on the hydration of Portland cements. Cem Concr Res 2008;38(6):848–60.
[40] Skalny J, Gebauer J, Odler I, editors. Material science of concrete, special volume: calcium hydroxide in concrete. The American Ceramic Society, Westerville; 2001.
[41] Laugesen JL. Density functional calculations of elastic properties of portlandite, Ca(OH)(2). Cem Concr Res 2005;35(2):199–202.
[42] Speziale S, Jiang F, Mao Z, Monteiro PJM, Wenk H-R, Duffy TS, Schilling FR. Single-crystal elastic constants of natural ettringite. Cem Concr Res 2008;38(7):885–9.
[43] Garboczi EJ, Day AR. An algorithm for computing the effective linear elastic properties of heterogeneous materials: 3D results for composites with equal phase Poisson ratios. J Mech Phys Solids 1995;43:1349–62.
[44] Arns CH, Knackstedt MA, Val Pinczewski W, Garboczi EJ. Computation of linear elastic properties from microtomographic images. J Geophys 2002;67:1396–405.
[45] Ulm FJ, Vandamme M, Bobko C, Ortega JA, Tai K, Ortiz C. Statistical indentation techniques for hydrated nanocomposites: concrete, bone, and shale. J Am Ceram Soc 2007;90(9):2677–92.
[46] Pharr GM, Oliver WC. Measurement of thin-film mechanical-properties using nanoindentation. MRS Bull 1992;17:28.
[47] Plassard C, Lesniewska E, Pochard I, Nonat A. Investigation of the surface structure and elastic properties of calcium silicate hydrates at the nanoscale. Ultramicroscopy 2004;100(3–4):331–8.